(Article begins on next page)

Corresponding Author: Dr. Gianni Barucca, PhD

Corresponding Author's Institution: University

First Author: Gianni Barucca, PhD

Order of Authors: Gianni Barucca, PhD; Eleonora Santecchia; Giuseppe Majni; Emmanuelle Girardin; Elena Bassoli; Lucia Denti; Andrea Gatto; Luca Iuliano; Tomasz Moskalewicz; Paolo Mengucci

Abstract: Direct Metal Laser Sintering (DMLS) is a technique to manufacture complex functional mechanical parts from a computer-aided design (CAD) model. Usually, the mechanical components produced by this procedure show higher residual porosity and poorer mechanical properties than those obtained by conventional manufacturing techniques.
In this work, a Co-Cr-Mo alloy produced by DMLS with a composition suitable for biomedical applications was submitted to hardness measurements and structural characterisation. The alloy showed a hardness value remarkably higher than those commonly obtained for the same cast or wrought alloys. In order to clarify the origin of this unexpected result, the samples microstructure was investigated by X-ray diffraction (XRD), electron microscopy (SEM and TEM) and energy dispersive microanalysis (EDX). For the first time, a homogeneous microstructure comprised of an intricate network of thin ε (hcp)-lamellae distributed inside a γ (fcc) phase was observed. The ε-lamellae grown on the {111}γ planes limit the dislocation slip inside the γ (fcc) phase, causing the measured hardness increase. The results suggest possible innovative applications of the DMLS technique to the production of mechanical parts in the medical and dental fields.

Highlights

- Samples of a Co-Cr-Mo biomedical alloy were produced by direct metal laser sintering.

- Samples show hardness values unexpectedly high.

- Samples were investigated by X-ray diffraction and electron microscopy techniques.

- A fine structure composed of ε-phase lamellae formed inside the γ-phase was observed.

- The correlation between microstructure and mechanical properties was identified.

- Results suggest important applicative potential of the production technique in the medical field.

1 # Structural characterization of biomedical Co-Cr-Mo

2 # components produced by Direct Metal Laser Sintering

3

4 G. Barucca [a,*], E. Santecchia [a], G. Majni [a], E. Girardin [b], E. Bassoli [c], L. Denti [c], A. Gatto [c],

5 L. Iuliano [d], T. Moskalewicz [e], P. Mengucci [a]

6

7 [a] SIMAU, Università Politecnica delle Marche, via Brecce Bianche, 60131 Ancona, Italy.

8 [b] DISCO, Università Politecnica delle Marche, via Brecce Bianche, 60131 Ancona, Italy.

9 [c] DIMeC, University of Modena and Reggio Emilia, via Vignolese 905/B, Modena 41125, Italy.

10 [d] DISPEA, Politecnico di Torino, C.so Duca degli Abruzzi 24, 10129 Torino, Italy.

11 [e] Faculty of Metals Engineering and Industrial Computer Science, AGH University of Science

12 and Technology, Al. Mickiewicza 30, 30-059 Kraków, Poland.

13

14

15 [*] Corresponding author: SIMAU, Università Politecnica delle Marche, via Brecce Bianche,

16 60131 Ancona, Italy. Tel.: +39 071 2204754; fax: +39 071 2204729.

17 E-mail address: g.barucca@univpm.it (G. Barucca).

Highlights

19 • Samples of a Co-Cr-Mo biomedical alloy were produced by direct metal laser sintering.

20 • Samples show hardness values unexpectedly high.

21 • Samples were investigated by X-ray diffraction and electron microscopy techniques.

22 • A fine structure composed of ε-phase lamellae formed inside the γ-phase was observed.

23 • The correlation between microstructure and mechanical properties was identified.

24 • Results suggest important applicative potential of the production technique in the medical

25 field.

26   **ABSTRACT**

27   Direct Metal Laser Sintering (DMLS) is a technique to manufacture complex functional

28   mechanical parts from a computer-aided design (CAD) model. Usually, the mechanical

29   components produced by this procedure show higher residual porosity and poorer mechanical

30   properties than those obtained by conventional manufacturing techniques.

31   In this work, a Co-Cr-Mo alloy produced by DMLS with a composition suitable for biomedical

32   applications was submitted to hardness measurements and structural characterisation. The alloy

33   showed a hardness value remarkably higher than those commonly obtained for the same cast or

34   wrought alloys. In order to clarify the origin of this unexpected result, the samples microstructure

35   was investigated by X-ray diffraction (XRD), electron microscopy (SEM and TEM) and energy

36   dispersive microanalysis (EDX). For the first time, a homogeneous microstructure comprised of

37   an intricate network of thin ε (hcp)-lamellae distributed inside a γ (fcc) phase was observed. The

38   ε-lamellae grown on the $\{111\}_\gamma$ planes limit the dislocation slip inside the γ (fcc) phase, causing

39   the measured hardness increase. The results suggest possible innovative applications of the

40   DMLS technique to the production of mechanical parts in the medical and dental fields.

41

42

43   **KEYWORDS**:   metals and alloys; laser processing; sintering; transmission   electron

44   microscopy, TEM; scanning electron microscopy, SEM; X-ray diffraction.

45

1. INTRODUCTION

Nowadays, a new class of manufacturing methods are becoming increasingly important for the production of biomedical devices. Among them, novel methods based on additive manufacturing (AM), assisted by computer-aided design/computer-aided manufacturing (CAD/CAM), allow the production of intricate mechanical parts [1-4].

Direct metal laser sintering (DMLS) is an AM process that uses the heat of a solid state laser to sinter metal powder particles [5]. In this case, a distribution mechanism pre-places successive layers of powder on a suitable substrate, while a laser beam controlled by a scanning system locally sinters the powder in accordance with the CAD model [6]. This technology, like other AM procedures, is highly rewarding in medicine where a high degree of personalization is required [7-9]. Prosthetic applications are particularly well suited for processing by means of DMLS due to their complex geometry, low volume and strong individualization [10]. Furthermore, the manufacturing of multiple unique parts in a single production run enables extensive customization with a strong reduction of manual operation leading to higher repeatability and good savings in money and delivery times.

Cobalt-based alloys were extensively used in cast and hard facing forms over the past twenty years because of their corrosion and wear resistance, biocompatibility and excellent strength and toughness at high temperature [11]. Typical applications of the Co-based alloys involved both the biomedical and the metallurgical fields [12, 13].

From a structural point of view, cobalt is characterized by a ε (hcp) low temperature phase and a γ (fcc) phase at higher temperature. The addition of chromium improves the corrosion and the oxidation resistance of the alloy, as well as its hardness, ductility and wear resistance through

4

68 carbide formation. Molybdenum improves the corrosion resistance and acts as a solid-solution

69 strengthener by forming the Co_3Mo (hcp) intermetallic compound [14].

70 Cast alloys with a Cr content ranging from 19 wt% to 30 wt% and a Mo content in the range 5-

71 10 wt% were considered for biomedical applications and for many years these compositions

72 were used to produce medical implants such as hips, knees, ankles and bone plates [15].

73 Although in the past few years, several AM techniques were applied to produce biocompatible

74 Co-based alloys, only in few cases a deep microstructural characterisation of the sintered

75 components were performed. In particular, Gaytan et al. reported on the microstructure and the

76 mechanical properties of Co-based prototypes produced by electron beam melting. In this study,

77 they found high hardness values attributed to the formation of an ordinate array of metal carbides

78 [16]. Meacock et al. investigated the microstructure and the mechanical properties of a

79 biomedical Co-Cr-Mo alloy produced by laser powder microdeposition [17]. They observed a

80 homogenous microstructure comprised of fine cellular dendrites and measured an average

81 hardness value of 460 HV_{02}, well higher than the typical values obtained by other fabrication

82 processes. From these results, they concluded that the fine morphology is responsible of the

83 significantly increased hardness value.

84 Few other papers deal with the possibility of realizing medical parts of a Co-Cr-Mo alloy by

85 DMLS, but it is worth to note that none of them reports the correlation of the samples

86 microstructure to the mechanical properties of the final components [19-21].

87 The mechanical properties of the sintered components are strictly linked to the samples

88 microstructure and are one of the major aspects connected to the practical applications of the AM

89 procedures. Usually, objects produced by metal powder sintering show poorer mechanical

90 properties than those produced by conventional procedures. This behaviour is mainly due to the

91 fact that DMLS, depending on the laser energy density employed, involves a partial or total

92 melting of the powder. Therefore, the products made by DMLS could show high surface

93 roughness, porosity (in certain cases even lack of densification), heterogeneous microstructure

94 and thermal residual stresses, that may give rise to poor mechanical properties [22].

95 In this paper, metallic components of a biocompatible Co-Cr-Mo alloy produced by the DMLS

96 technique were deeply investigated in order to correlate their mechanical properties to the

97 corresponding microstructure. To this aim, hardness measurements, X ray diffraction (XRD)

98 analysis, electron microscopy (SEM, TEM) observations and energy dispersive microanalysis

99 (EDX) were performed on the samples. Results evidenced a surprisingly high hardness value of

100 the investigated Co-Cr-Mo alloy in comparison of the hardness values commonly reported in

101 literature for similar compositions. This unexpected result was attributed to the peculiar

102 microstructure observed in the analysed samples, that, to our knowledge, was never reported

103 before.

104

105 **2. MATERIALS AND METHODS**

106 *2.1 Material composition and sintering parameters*

107 Specimens were prepared by direct metal laser sintering using a Yb (ytterbium) fiber laser

108 system (EOSINT-M270) operating with the standard deposition parameters reported in Table1.

109 **Table 1.** *Parameters used for DMLS*

laser power	200W
laser spot diameter	0.200 mm
Scan speed	up to 7.0 m/s
Building speed	2-20 mm^3/s
Layer thickness	0.020 mm
Protective atmosphere	max 1.5% oxygen

110

111 A Co-Cr-Mo alloy powder (EOS Cobalt/Chrome SP2) with the nominal composition (in wt%)

112 Co 63.8, Cr 24.7, Mo 5.1, W 5.4 , Si 1.0, was used as raw material. The powder if free of Ni, Be

113 and Cd according to EN ISO 22674. The nominal composition was provided by the manufacturer

114 (EOS GmbH Electro Optical Systems). The powder is the EOS Cobalt/Chrome SP2 cobalt based

115 metal ceramic alloy intended for production of Porcelain-Fused to Metal (PFM) dental

116 restorations (crowns, bridges, etc.) in EOSINT M 270 Standard installation mode. The powder is

117 class IIa medical device in accordance with annex IX rule 8 of the MDD 93/42/EEC.

118 Composition corresponds to "type 4" CoCr dental material according to EN ISO 22674.

119 Rectangular parallelepipeds with size 250 mm x 4 mm and a thickness of 6 mm were sintered by

120 using the parameters reported in Table 1. In order to minimize anisotropy, each layer was built

121 with the laser scanning along a specific direction. Layer-by-layer the scanning direction was

122 rotated by 25° with respect to the previous one.

123

124 *2.2 Hardness measurements*

125 Hardness tests were performed on the sintered samples using the Rockwell scale C

126 (specifications ISO 4498 : Sintered metal materials, excluding hard metals - Determination of

127 apparent hardness and microhardness). Measurements were obtained averaging five indentations

128 following ISO 6508: Rockwell hardness test.

129

130 *2.3 Structural characterisation*

131 Structural and microstructural characterizations were carried out by X-ray diffraction (XRD),

132 scanning (SEM) and transmission (TEM) electron microscopy techniques.

133 XRD measurements were performed by a Bruker D8 Advance diffractometer operating with a

134 Cu-Kα radiation source at V= 40kV and I= 40 mA in the angular range $2\theta = 10 - 90°$.

135 SEM analyses were carried out by a ZEISS SUPRA 40 microscope equipped with a Bruker

136 Quantax energy dispersive X-ray microanalysis (EDX). Observations were performed on both

137 the as-received metallic powder and cross-sectioned sintered samples. Before observations,

138 samples surfaces were prepared using a conventional metallographic procedure and

139 electrochemically etched in the following conditions: HCl 0.1 M, 2V, 2 min.

140 TEM analyses were carried out by a Philips CM200 electron microscope operating at 200 kV

141 and by a JEOL JEM-2010 ARP microscope equipped with an Oxford Inca energy dispersive X-

142 ray microanalysis (EDX). For TEM observations, samples were prepared by the conventional

143 thinning procedure consisting of mechanical polishing by grinding papers, diamond pastes and a

144 dimple grinder. Final thinning was carried out by an ion beam system (Gatan PIPS) using Ar

145 ions at 5 kV.

146

147 **3. RESULTS**

148   *3.1 Hardness*

149   The average Rockwell C hardness (HRC) value measured for the laser sintered samples is 47

150   HRC, a very high value considering that the usual range for cast Co-Cr-Mo alloys is from 25 to

151   35 HRC.

152

153   *3.2 X-ray diffraction (XRD)*

154   X-ray diffraction measurements were performed on both the Co-Cr-Mo powder used as raw

155   material for the DMLS process and on the different regions of the sintered samples (Fig. 1).
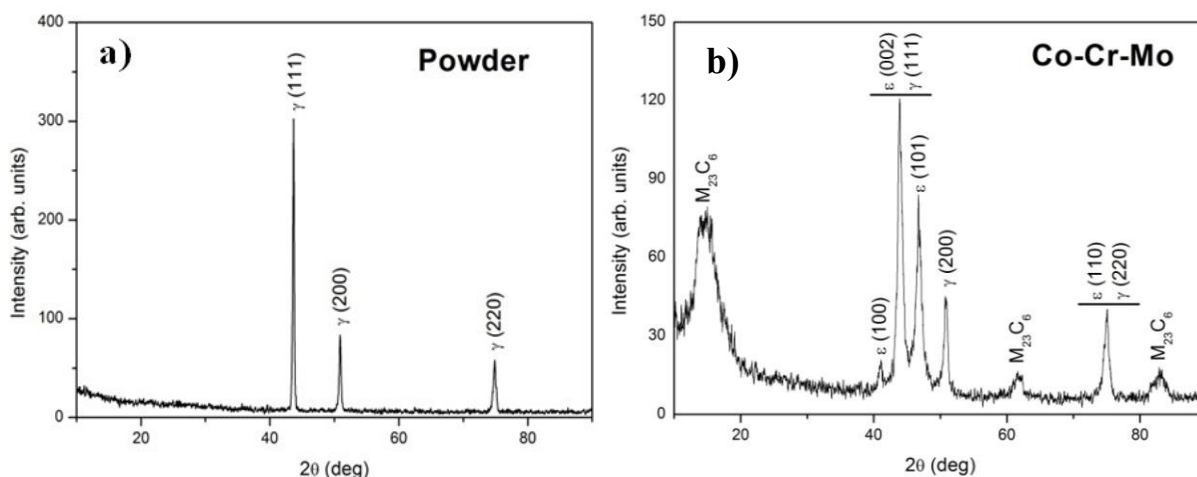
156   **Fig. 1.** *X-ray diffraction patterns: a) as-received metallic powder; b) sintered sample.*

157

158   Fig. 1a reports the XRD pattern of the as-received metallic powder. All the visible peaks can be

159   attributed to the cubic cobalt phase, commonly referred to as γ phase. The γ phase has a face

160   centred cubic (fcc) lattice with a nominal parameter a=0.35447 nm (ICDD card n. 15-806). For

161   the alloy under study, the best fit performed by using the three diffraction peaks of Fig. 1a

162   provides a lattice parameter value a=0.3586 nm, in close agreement with the values reported in

163   literature for alloys of similar composition [23].

164   The XRD pattern of the sintered sample is shown in Fig. 1b. The most intense and well-defined

165   peaks are a result of the simultaneous presence of both γ and ε cobalt phases, as indicated in Fig.

166   1b where each diffraction peak is indexed with the name of the corresponding Co phase. A

167   double indexation is reported for the most intense peak at $2\theta=43.94°$ and the peak at $2\theta=75.09°$

168   because of the superposition of the reflections due to the ε and γ phases. The ε phase has a

169   hexagonal close packed (hcp) lattice with nominal parameters a=0.25031 nm and c=0.40605 nm

170   (ICDD card n. 5-727). By using the ε (100) and ε (101) peaks of the XRD pattern shown in Fig.

171   1b, the lattice parameters of the hexagonal ε phase formed in our alloy were determined to be

172   a=0.2539 nm and c=0.4122 nm with a c/a ratio of 1.623. The lattice parameter of the fcc γ phase

173   formed in the sintered sample evaluated by the γ (200) peak of Fig. 1b is a=0.3589 nm. Also in

174   this case, the calculated lattice parameters for the ε and γ phases formed in our alloy are in close

175   agreement with those reported in literature for similar compositions [23].

176   In order to estimate the volume fraction of the hcp and fcc cobalt phases in the sintered sample,

177   the integrated intensities of the γ (200) and ε (101) peaks were used. The quantitative

178   determination, performed by using the method of Sage and Gillaud [24], resulted in an ε-phase

179   volume fraction f_{hcp}=0.49±0.03.

180   In addition to the ε and γ peaks in Fig. 1b, three broad peaks attributable to metals carbides are

181   also visible. These latter peaks generically indexed as $M_{23}C_6$ (M=Cr, Co, Mo, W) are due to

182   metal carbides having the cubic structure of the $Cr_{23}C_6$ compound (ICDD card n. 35-783).

183

184   *3.3 Scanning electron microscopy (SEM) and microanalysis (EDX)*

185   Scanning electron microscopy observations were performed on the as-received powder and on

186   the sintered samples. Particles forming the metallic powder are shown in Fig. 2.

187 From the SEM images the average size of the spherical particles were evaluated. Measurements

188 were performed by averaging the data obtained from different areas of the samples. Results

189 showed that the size of the particles ranges from 4 to 80 μm.
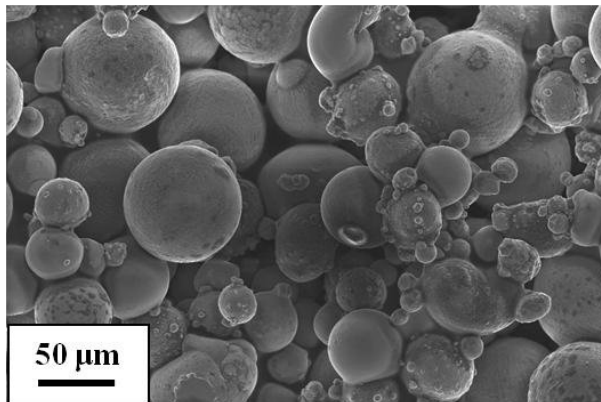
190 **Fig. 2.** *SEM image of the as-received metallic powder.*

191 EDX analysis performed on the powder showed a chemical composition in agreement with the

192 nominal composition of the alloy reported above. In Table 2 the experimental values obtained

193 from the EDX analyses performed on the powder and on the sintered sample are reported.

194

195 **Table 2.** *Experimental results of the EDX microanalysis performed on both the powder and the*

196 *sintered sample.*

Element	Powder (wt%)	Sintered sample (wt%)
Co	62	63
Cr	26	26
Mo	5	6
W	4	4
Si	1	1

197

198   It is worth to note that the average composition of the powder and the sintered sample is almost

199   the same, as can be inferred from Table 2.

200   The inner structure of the sintered samples, as observed by SEM, is shown in Fig. 3. Samples

201   were sectioned parallel to the laser beam direction, and SEM observations were performed after

202   a metallographic preparation of the surfaces followed by an electrochemical etching. The lines

203   separating the different weld pools produced by the laser scan on each layer are evidenced by

204   arrows in the image taken at low magnification, Fig. 3a.
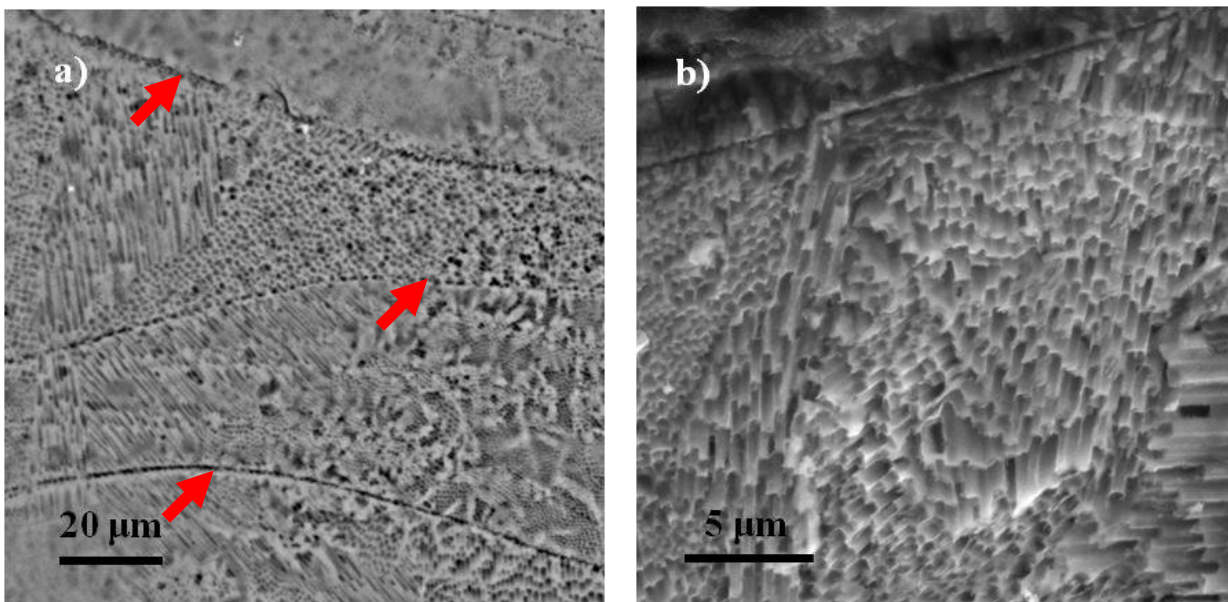
205   **Fig. 3** *SEM images of the sintered samples. a) low magnification: lines separating different weld*

206   *pools are arrowed; b) high magnification.*

207

208   Observations performed at higher magnification allow to evidence the presence of an extremely

209   fine microstructure inside a single pool, Fig. 3b. Columnar structures, with diameters ranging

210   from 300 to 400 nm and heights from 4 to 8 μm, grow inside the matrix in form of domains. The

211   orientation of the columns is the same inside a single domain while it changes from one domain

212   to the other. In order to estimate the area fraction occupied by the columnar structures relative to

12

213   the matrix, several SEM images were processed by using an image analysis software [25]. An

214   area fraction of 45±5% was provided by software. This value, as a rough approximation, can be

215   considered as the volume fraction of the columnar structures relative to the rest of the sample.

216

217   *3.4 Transmission electron microscopy (TEM) and microanalysis (EDX)*

218   TEM observations of the sintered samples confirm the presence of the two ε and γ cobalt phases.

219   The ε phase forms as small lamellae inside the γ phase. The thickness of the ε phase lamellae is

220   1-2 nm, but in some cases, they tend to aggregate in the same region of the sample forming

221   alternate structures of ε and γ phases with lateral dimensions of up to 400 nm.

222
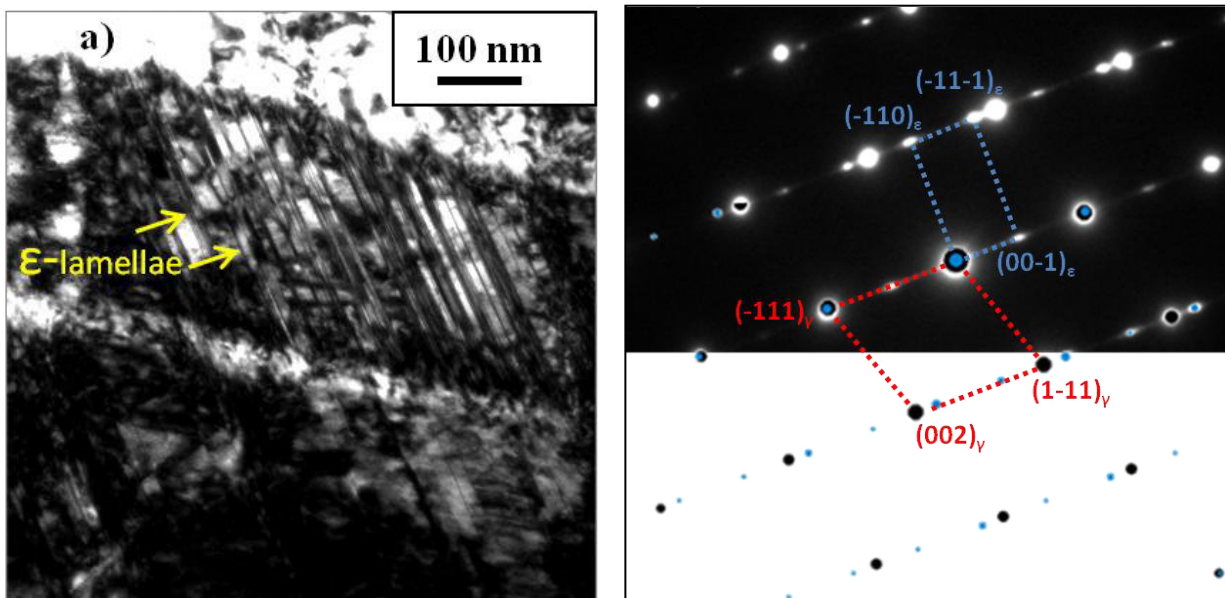
223   **Fig. 4.** *Sintered sample: a) TEM bright field image of the ε lamellae inside the γ phase*

224   *(arrowed); b) SAD pattern taken in the same area in <110>γ zone axis orientation (upper part)*

225   *and corresponding software simulation (lower part). In red is indicated the cell of the γ-Cobalt*

226   *phase and in blue the cell of the ε-Cobalt phase.*

227

228 In Fig. 4a, taken in $<110>_\gamma$ zone axis orientation, the lamellar structure is clearly visible. The

229 lamellae are parallel to each other, and the distance between them is not constant. Considering

230 the ensemble of these lamellae, it is possible to envisage one of the columnar structures visible in

231 the SEM images. The corresponding selected area diffraction (SAD) pattern is reported in the

232 upper part of Fig. 4b while its simulation performed with the CrystalKitX software [26] is shown

233 in the lower part of Fig. 4b. The remarkable agreement between the simulated pattern and the

234 experimental one is evident. The most intense spots visible in Fig. 4b (top) are a result of the fcc

235 γ-phase (red cell) while the smaller ones are a result of the hcp ε-phase (blue cell). The geometry

236 of the spot distribution in the SAD pattern of Fig. 4b (top) reveals that the ε lamellae form with

237 the following orientation relationships with the γ matrix:

238 $$\{001\}_\varepsilon \mathbin{/\!/} \{111\}_\gamma$$

239 $$<100>_\varepsilon \mathbin{/\!/} <1\text{-}10>_\gamma$$

240 Furthermore, as can be observed in Fig. 4b (top), the spots of the ε phase are streaked in direction

241 of the $\{111\}_\gamma$ spots indicating that the lamellae grow on the $\{111\}_\gamma$ lattice planes and have a

242 small thickness in the $<111>_\gamma$ lattice direction.

243 In order to investigate the spatial distribution of the hcp lamellae in greater details, TEM

244 observations were also performed in the $<111>_\gamma$ zone axis orientation.

14
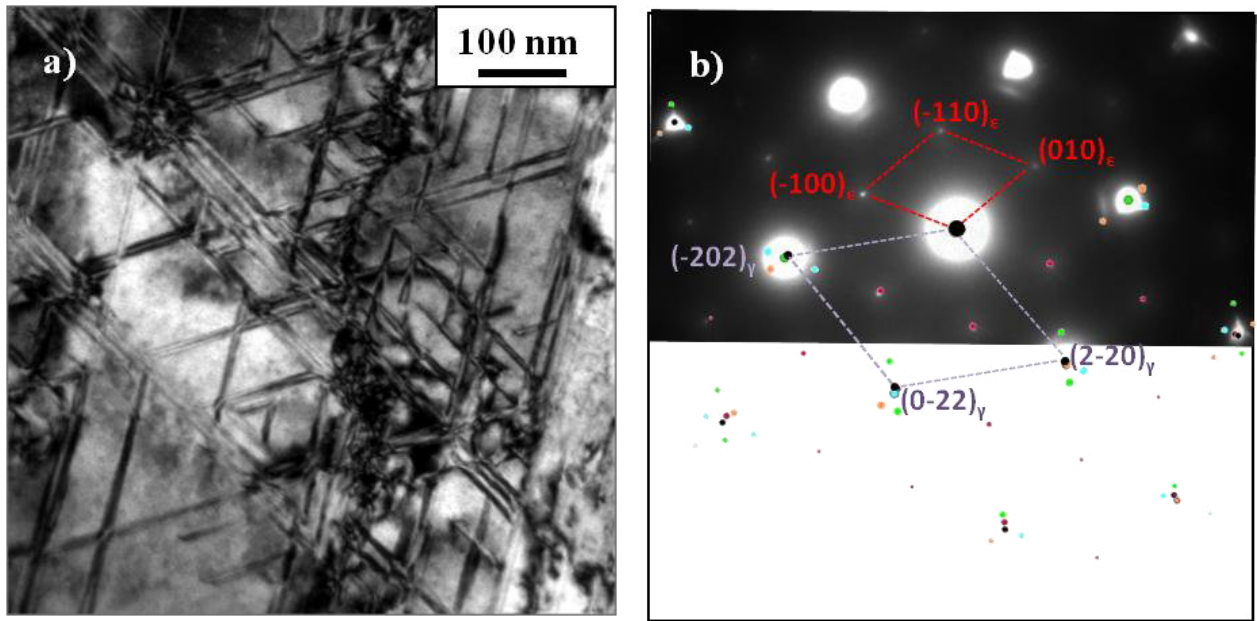
Fig. 5. *Sintered sample: a) bright field TEM image taken in <111>$_\gamma$ zone axis orientation; b) corresponding SAD pattern (upper part) and software simulation (lower part). In red is indicated the cell of the ε-Cobalt phase in one of the four possible orientations on the {111}$_\gamma$ lattice planes, and in violet the cell of the γ-Cobalt phase.*

A bright field image of the sample in this orientation is shown in Fig. 5a. Lamellae and stacking faults lying on different {111}$_\gamma$ lattice planes are visible and form an intricate network. The corresponding SAD pattern, with the simulation performed by the CrystalKitX software, are shown in the upper and lower part of Fig. 5b, respectively. The SAD pattern was simulated considering the four possible orientations of the ε phase on the {111}$_\gamma$ lattice planes. Different colours correspond to different orientations. In particular the diffraction spots corresponding to the (001)$_\varepsilon$ // (111)$_\gamma$ orientation were indexed in Fig. 5b and indicated with the red cell.

It must be stressed that all the SAD patterns, taken even in other orientations, never showed the presence of twins reflections (1/3 <hkl>), although at a first glance the ε lamellae could be confused with microtwins.

15

260 TEM observations performed on the sintered samples also revealed the presence of small

261 quantities of precipitates uniformly distributed. Precipitates, visible as dark dots inside the matrix

262 in Fig. 6, have a spherical or elliptical shape with size ranging from 50 to 300 nm.
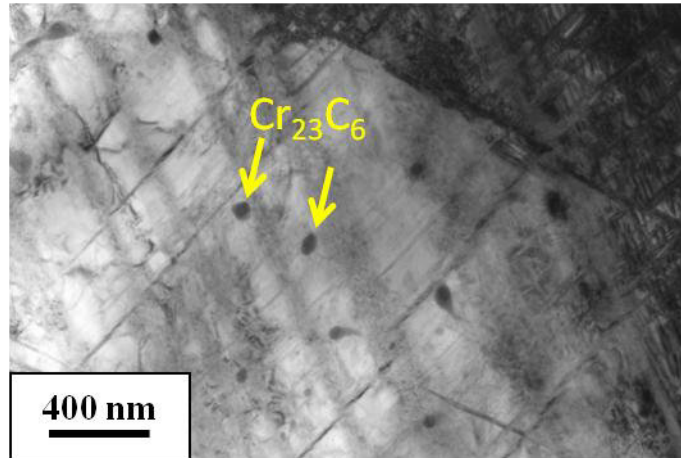
263 **Fig. 6.** *TEM bright field image of the sintered sample showing the presence of some metal*

264 *carbides (arrowed).*

265

266 In order to investigate the chemical composition of these precipitates, EDX measurements were

267 performed. Results show an increase of the Cr, W and Mo content in the precipitates with respect

268 to the matrix, while the precipitates composition remains almost the same independently of their

269 shape, Table 3. The crystallographic nature of the precipitates was investigated by the SAD

270 technique. Results are compatible with the presence of a phase having the $Cr_{23}C_6$ lattice

271 structure.

16

Table 3. *Experimental results of the EDX measurements performed on both the matrix and the precipitates.*

Element	Matrix (wt%)	Precipitates (wt%)
Co	63	52
Cr	24	26
Mo	5	11
W	6	10
Si	1	1

4. DISCUSSION

The hardness values of the laser sintered samples are surprisingly high, considering the method used for their realization. Generally, components produced by an additive manufacturing technique, such as the Direct Laser Metal Sintering procedure used in this work, can be affected by residual porosity and show poorer mechanical properties than those obtained by traditional manufacturing techniques [22]. In our case, however, hardness results to be remarkably high, even if compared to the same cast or wrought alloy. The explanation of this result is linked to the inner structure of the samples, as will be discussed below. Furthermore, it must be stressed that hardness is only one of the mechanical properties playing an important role in material selection for application in the human body [12]. Other quantities such as tensile strength, Young's modulus and elongation must be considered when the application range of a biomaterial is involved. On the other hand, Murr et al. demonstrated the possibility to set the Young's modulus of femoral component constituted of a Co-29Cr-6Mo alloy by opportunely developing mesh and

17

288   foam implant prototypes produced by an additive manufacturing technique [27]. This means that

289   the implant design influences also its final mechanical properties.

290   X-ray diffraction results show a phase transformation connected to the laser treatment. In

291   particular, while the powder is exclusively composed of the γ (fcc) cobalt phase, the sintered

292   sample contains both the γ (fcc) and ε (hcp) phases. Cobalt-based alloys undergo an fcc $\leftrightarrow$ hcp

293   martensitic transformation. The equilibrium temperature between the high-temperature γ (fcc)

294   phase and the low-temperature ε (hcp) phase is around 970 °C. In pure Co the equilibrium

295   temperature between the two phases is around 427°C [28]. The fcc $\rightarrow$ hcp transformation in Co

296   and its alloys is very sluggish due to the limited chemical driving forces available at the

297   transformation temperature. Thus, under normal cooling conditions, the fcc phase is retained

298   below the phase boundary in a metastable state. The metastable fcc phase can transform to hcp

299   by plastic deformation, by isothermal aging at temperatures between 650 and 950 °C, and

300   athermally, by rapid cooling from the annealing temperatures (> 1100°C) [24,29]. In our

301   samples, the laser beam produces the local melting of the metal powder that rapidly solidifies

302   and cools down due to the high thermal conductivity of the metallic alloy and the smallness of

303   the heated area during the laser treatment. Thus, in the successive small areas treated with the

304   laser beam during the production process is possible to reach a condition very similar to that

305   responsible of the athermal martensitic transformation. Accordingly the athermal martensitic

306   transformation is the origin of the ε (hcp) phase in our sintered samples.

307   SEM observations of the DLMS samples, reveal a complex microstructure. Parallel columnar

308   structures form different domains inside the same melted pool produced by the laser beam. This

309   morphology is very different from the cellular dendritic morphology observed by Meacock et al

310   [17]. They reported on the microstructure and properties of a typical Co-Cr-Mo biomedical alloy

311   manufactured by laser powder microdeposition (LPMD). Although this latter technique,

312   similarly to the DLMS, involves melting of a small quantity of metal powder by a laser beam

313   followed by a rapid quenching, different microstructures are produced. It must be stressed that

314   the laser sintering process is very complex because it involves multiple modes of heat, mass and

315   momentum transfer, and chemical reactions [5]. As a consequence, it is not too surprising that

316   two different laser sintering techniques produce different final samples microstructure. Gaytan et

317   al. [16] reported on the microstructure and mechanical properties of parts fabricated by electron

318   beam melting (EBM) of a Co-26Cr-6Mo-0.2C powder. They observed hardness values similar to

319   the values experimentally obtained in our work, attributed to the formation of carbides lined up

320   to form columns perpendicular to the build direction. Although the columns of carbides look

321   similar to the columnar structures visible in our SEM images, XRD and TEM analyses show that

322   metal carbides are only present in small quantities and do not form columnar structures in our

323   samples. In particular, TEM observations reveal the formation of ε-martensite lamellae inside the

324   fcc-Co grains. These lamellae grow on the {111} planes of the cubic γ-phase and tend to

325   aggregate forming the columnar structures visible in the SEM images. Therefore, the columnar

326   structures visible in our SEM images although similar to other structure reported in literature,

327   have a completely different nature, never observed before.

328   As known, the hcp stacking sequence can be produced by introducing an intrinsic stacking fault

329   on every second (111) plane of an fcc lattice. Furthermore, this can be accomplished by a

330   shearing process if the intrinsic faults are bounded by Shockley a/6 <112> partial dislocations.

331   This mechanism, invoked in the fcc→hcp martensitic transformation [30], explains the

332   orientation relationship between the ε and the γ phases experimentally observed in the electron

333   diffraction patterns reported in Fig. 4b. Considering the different families of {111} planes, the

334   presence of different orientations of the columnar structures inside a single melt pool is not

335   surprising.

336   The estimation of the area fraction occupied by the columnar structures with respect to the

337   matrix, obtained by SEM images elaboration, is comparable with the ε-phase volume fractions

338   obtained by XRD spectra analyses. This is in agreement with TEM observations revealing that

339   the columnar structures are due to the aggregation of ε-martensite lamellae.

340   Generally, for a conventional Co-Cr-Mo alloy, the percentage of athermal ε-martensite ranges

341   from 10 vol.% to 15vol.% depending on the chemical composition of the alloy, the solution

342   temperature and time, and the cooling rate [28]. Using only conventionally [31] or laser sintered

343   [17] Co-Cr-Mo powders, amounts of athermal ε-martensite ranging from 30 vol.% to 70 vol.%

344   were produced. The reason for these large amounts was mainly attributed to a large nucleation of

345   ε-embryos promoted by the free surfaces and grain development at powder contact surfaces

346   combined with recrystallization and grain growth within the powder particles, or promoted by

347   the cell grain boundary between the dendritic and interdendritic zone. In our samples, the cellular

348   dendritic morphology was not observed, and the powder particles completely melted during the

349   laser treatment. Thus, it is not possible to invoke in our samples the same mechanisms of

350   nucleation promotion. Furthermore, in the two above-mentioned works, TEM analyses were not

351   performed, therefore it is not possible to compare the distribution and morphology of the ε-

352   phase. Comparisons can be performed with the athermal ε-martensite present in conventional

353   Co-Cr-Mo alloys [32]. In such case, the ε-phase forms thick bands inside the fcc-phase. To our

354   knowledge, the formation of an intricate network of thin ε-lamellae, comparable to that of our

355   samples, was never observed before. All this suggests that in the DLMS procedure the cooling

356   rates of the melted powder are so rapid that a lot of lattice defects are formed during

357 solidification, and these defects exactly represent the ε-embryos promoting the martensitic

358 transformation.

359 For completeness, during the samples sintering, the deposited layers were heated as each

360 successive layer was deposited. These heating treatments could have induced isothermal

361 martensitic transformations in the alloy. However, it is reported in literature that the isothermal

362 martensitic formation is accompanied by the formation of discontinuous rows of carbides

363 connected to the negligible carbon solubility in the hcp phase [30,33]. The spherical carbides

364 present in our samples do not satisfy the features reported above, and they are probably formed

365 during the solidification process.

366 The HRC hardness values reported for the common cast Co-Cr-Mo alloys range from 25 to 35

367 HRC. These values are considerably lower than those measured in the part manufactured by

368 DLMS. Furthermore, it was found that the hardness value exhibits a linear increase at the

369 increasing of the ε phase content [24]. This latter result can be attributed to the growth of the ε-

370 phase on the $\{111\}_\gamma$ planes that restrict dislocation slip in the fcc lattice. Moreover, the

371 dislocation slip in the hcp lamellae is also inhibited by the intersection of these hcp lamellae with

372 other hcp ones or with fcc regions [30]. Therefore, all the aforementioned phenomena and the

373 peculiar intricate network of ε-lamellae experimentally observed in our samples, can explain the

374 high hardness values obtained. In fact, in our samples the ε lamellae grow on the slip plains of

375 the γ-(fcc) phase. The density and the spatial distribution of these ε lamellae enormously restrict

376 the dislocations slip, thus increasing the hardness values of our samples.

377 The presence of metal carbides could even play a role in the strengthening of the alloy by the

378 Orowan mechanism. However, considering the small quantity of carbides observed in our

379 samples, it is more probable that the main mechanism of strengthening is due to the martensitic

380 transformation induced in the alloy by the DLMS procedure.

381 The increased strengthening manifested in the sintered samples along with the microstructure

382 homogeneity observed could make the direct metal laser sintering technique a very useful and

383 powerful procedure to produce surgical implants from Co-Cr-Mo alloys.

384 Future work will involve studies on the correlation between the deposition parameters of the

385 DMLS production process, and the microstructure and the mechanical properties of the final

386 products. Furthermore, additional mechanical tests will be performed on the sintered Co-Cr-Mo

387 samples in order to investigate tensile strength, Young's modulus and elongation.

388

389 **5. CONCLUSIONS**

390 In the present paper, we reported on the structural and microstructural characterization of Co-Cr-

391 Mo parts produced by Direct Metal Laser Sintering. The composition of the alloy was chosen in

392 order to produce biocompatible parts. Sintered samples were characterized by X-ray diffraction,

393 scanning and transmission electron microscopy and EDS microanalysis. The main results

394 obtained can be listed as follows:

395 1) The laser treatment melts the metallic Co-Cr-Mo powder and induces a phase transformation

396 from the γ (fcc) to the ε (hcp) phase;

397 2) The phase transformation is an athermal martensitic transformation and produces an intricate

398 network of thin ε-lamellae distributed inside the γ phase. This microstructure was never observed

399 before;

400 3) The large amount of ε-lamellae could be attributed to a large nucleation of ε-embryos

401 promoted by lattice defects formation during the rapid cooling of the melted powder;

402   4) Carbides are present inside the grains of the alloy and are probably formed on solidification;

403   5) The hardness values of the samples, higher than those reported in parts fabricated by different

404   processes, are due to the presence of ε-lamellae grown on the $\{111\}_\gamma$ planes that restricts the

405   dislocations slip in the γ (fcc) phase. Furthermore, slip in the ε-lamellae is inhibited by the

406   intersection of these hcp lamellae with other hcp lamellae or with fcc regions.

407   6) The DMLS technique could be used to realize surgical implants, where an high degree of

408   personalisation is required, saving money and time with respect to conventional procedures.

409

412

413   **REFERENCES**

414   [1] A. Mazzoldi. Selective laser sintering in biomedical engineering. Med Biol Eng Comput

415   2013;51:245-256.

416   [2] Lantada AD, Morgado PL. Rapid prototyping for biomedical engineering: current capabilities

417   and challenges. Annual Review of Biomedical Engineering 2012;14:73-96.

418   [3] Rosochowski A, Matuszak A. Rapid tooling: the state of the art. J Mater Process Technol

419   2000;106:191-198.

420   [4] Hunt JA, Callaghan JT, Sutcliffe CJ, Morgan RH, Halford B, Black RA. The design and

421   production of Co-Cr alloy implants with controlled surface topography by CAD-CAM method

422   and their effects on osseointegration. Biomaterials 2005;26:5890-5897.

423   [5] Simchi A. Direct laser sintering of metal powders: Mechanism, kinetics and microstructural

424   features. Mater Sci Eng A 2006;428:148-158.

425 [6] Bassoli E, Gatto A, Iuliano L. Joining mechanisms and mechanical properties of PA

426 composites obtained by selective laser sintering. Rapid Prototyp J 2012;18:100-108.

427 [7] Gibson I, Cheung LK, Chow SP, Cheung WL, Beh SL, Savalani M, Lee SH. The use of rapid

428 prototyping to assist medical applications. Rapid Prototyp J 2006;12:53-58.

429 [8] Wang X, Yan Y, Zhang R. Rapid prototyping as a tool for manufacturing bioartificial livers.

430 Trends in Biotechnology 2007;25:505-513.

431 [9] Butscher A, Bohner M, Hofmann S, Gauckler L, Muller R. Structural and material

432 approaches to bone tissue engineering in powder-based three dimensional printing. Acta

433 Biomaterialia 2011;7:907-920.

434 [10] Atzeni E, Iuliano L, Minetola P, Salmi A. Proposal of an innovative benchmark for

435 accuracy evaluation of dental crown manufacturing. Computers in Biology and Medicine

436 2012;42:548-555.

437 [11] Davis JR. Nickel, Cobalt and Their Alloys Materials Park (OH): ASM

438 INTERNATIONAL;2000.

439 [12] Nasab MB, Hassan MR, Sahari BB. Metallic biomaterials of knee and hip - a review.

440 Trends Biomater. Artif. Organs 2010;24(2):69-82.

441 [13] Malayoglu U, Neville A. Mo and W as alloying elements in Co-based alloy – their effects

442 on erosion – corrosion resistance. Wear 2005;259:219-229.

443 [14] Shin J, Doh J, Kim J. Effect of molybdenum on the microstructure and wear resistance of

444 cobalt-base Stellite hardfacing alloys. Surf Coat Technol 2003;166:117-126.

445 [15] Davis JR, Handbook of Materials for Medical Devices: ASM International; 2003:21-50

446 DOI: 10.1361/hmmd2003p013.

447 [16] Gaytan SM, Murr LE, Martinez E, Martinez JL, Machado BI, Ramirez DA, Medina F,

448 Collins S, Wicher RB. Comparison of Microstructures and Mechanical Properties of Solid and

449 Mesh Cobalt-base Alloy Prototypes Fabricated by Electron Beam Melting. Metall Mater Trans

450 A 2010;41:3216-3227.

451 [17] Meacock CG, Vilar R. Structure and properties of a biomedical Co-Cr-Mo alloy produced

452 by laser powder microdeposition. J Laser Appl 2009;21:88-95.

453 [18] Vandenbroucke B, Kruth JP. Selective laser melting of biocompatible metals for rapid

454 manufacturing of medical parts. Rapid Prototyp J 2007;13:196-203.

455 [19] Averyanova M, Bertrand P, Verquin B. Manufacture of Co-Cr dental crowns and bridges by

456 selective laser Melting technology. Virtual Phys Prototyp 2011;16:179-185.

457 [20] Reclaru L, Ardelean L, Rusu L, Sinescu C. Co-Cr material selection in prosthetic

458 restoration: laser sintering technology. Solid state phenomena 2012;188:412-415.

459 [21] Cotrut CM, Ciucã S, Miculescu F, Antoniac I, Târcolea M, Vrânceanu DM. The influence

460 of classical and modern manufacturing technologies on the properties of metal dental bridge.

461 Key engineering materials 2014;583:163-168.

462 [22] Sanz C, Navas VG. Structural integrity of direct metal laser sintered parts subjected to

463 thermal and finishing treatments. Journal of materials processing technology 2013;213:2126-

464 2136.

465 [23] Saldivar-Garcia AJ, Lopez HF. Temperature effects on the lattice constants and crystal

466 structure of a Co-27Cr-5Mo low-carbon alloy. Metall Mater Trans A 2004;35:2517-2523.

467 [24] Garcia JS, Medrano MA, Rodriguez AS. Formation of hcp martensite during the isothermal

468 aging of an fcc Co-27Cr-5Mo-0.05C orthopedic implant alloy. Metall Mater Trans A

469 1999;30:1177-1184.

470 [25] Rasband WS. ImageJ, U. S. National Institutes of Health, Bethesda, Maryland, USA,

471 http://imagej.nih.gov/ij/ 1997-2012.

472 [26] CrystalKitX version 1.9.1. Total Resolution LLC.

473 [27] Murr LE, Amato KN, Li SJ, Tian YX, Cheng XY, Gaytan SM, Martinez E, Shindo PW,

474 Medina F, Wicker RB. Microstructure and mechanical properties of open-cellular biomaterials

475 prototypes for total knee replacement implants fabricated by electron beam melting. J Mech

476 Behav Biomed Mater 2011;4:1396-1411.

477 [28] Saldìvar-Garcia AJ, Manì MA, Salinas RA. Effect of solution treatments on the fcc/hcp

478 isothermal martensitic transformation in Co-27Cr-5Mo-0.05C aged at 800°C. Scr Mater

479 1999;40:717-722.

480 [29] Lopez HF. Alloy developments in biomedical Co-base alloys for HIP implant applications.

481 Materials science forum 2013;736:133-146.

482 [30] Vander Sande JB, Coke JR, Wulff J. A Transmission Electron Microscopy Study of the

483 Mechanisms of Strengthening in Heat-Treated Co-Cr-Mo-C Alloys. Metall Trans A

484 1976;7A:389-397.

485 [31] Song CB, Park HB, Seong HG, Lòpez HF. Development of a thermal ε-martensite in

486 atomized Co-Cr-Mo-C implant alloy powders. Acta Biomaterialia 2006;2:685-691.

487 [32] Lee SH, Nomura N, Chiba A. Significant improvement in mechanical properties of

488 biomedical Co-Cr-Mo alloys with combination of N addition and Cr-enrichment. Mater Trans

489 2008;49:260-264.

490 [33] Rajan K, Vander Sande JB. Room temperature strengthening mechanisms in a Co-Cr-Mo-C

491 alloy. J Mater Sci 1982;17:769-778.

Ms. Ref. No.: MSEC-D-14-00284
Title: Structural characterization of biomedical Co-Cr-Mo components produced by Direct Metal Laser Sintering
Materials Science and Engineering C

Authors reply

The paper has been revised following the reviewers suggestions. In particular, Abstract and Introduction were deeply modified.
English was checked throughout the manuscript.
A Highlights session is added in the manuscript.
In the following, the reviewer comment is indicated by "R:" while the authors reply by "A:".
The position of the text added or modified in the manuscript is specified in parentheses in terms of page number (p.) and line number (l.).

Reviewer #1: The authors present a paper aiming to analyze the hardness and the microstructure of samples produced by direct metal laser sintering of a Co-Cr-Mo alloy. I would propose Major Revisions.

R: In general terms, more clarity about the purpose of the work, how it fits into previous work and a clear evaluation of the outcomes is required. The author must emphasize why the paper provides new insight and it is interesting for the scientific community. A better connexion with previous research is also required to support the obtained results and place them into the context of literature.
A: Introduction has been deeply modified following the reviewer suggestions. New and updated references have been added [20, 21]. The original results presented in the paper are summarised both in the Abstract (p. 3, l. 36-40) and in the Introduction (p. 6, l. 95-103).

R: A gap of research has been identified when it is said that the 'The study of the samples microstructure is fundamental to set the parameters used in the AM procedures and to choose the composition of the metal powders in order to meet the request for certain mechanical properties'. However, no correlation between the obtained results and the parameters of the process and composition of the metal powders has been established. In order to make a contribution to knowledge, more concise statements should be stated describing the influence of the process on the material properties (hardness and microstructure), and some ways to mitigate the associated problems.
A: This part was deleted because not strictly focused on the subject matter. More information on the influence of the deposition parameters on the properties of the obtained components can be found in ref [22].

R: The language and writing style should aim to be concise, with simple, easy to understand sentences. The English needs to be checked throughout. Some sections should be divided in different subsections, such as 'Section 2' and 'Results'. This will simplify and clarify the text, and it will solve readability issues.

A: Language and writing style have been checked and revised throughout the document. Section 2 "Materials and methods" and Section 3 "Results" have been divided in subsections, as suggested.

R: Further remarks to the paper:
- Abstract: it should only report on experimental details, results and main conclusions. Including background information, such as the description of the Direct Metal Laser Sintering Technique, should be avoided.

A: Abstract has been modified, as suggested (p.3).

R: - English needs to be checked to avoid some language issues such as: 'objects realized by sintering metal powder…'; 'founded' instead of found (line 3, page 5); '…the mechanical properties was identified…', instead of 'were identified'.

A: English checked throughout the manuscript.

R: - Introduction section: although the authors summarize some previous work in the area, the context needs to be more convincingly presented, placed into the context of the literature. Please, cite more references on the production of Cr-Co-Mo samples by laser sintering and improve the explanation on the applicability of the research results in the biomedical field.

A: Introduction revised and more references added, as reported above (p. 4-6).

R: - Page 4, first paragraph. The author states that 'Recently, they have been attracting strong interest for biomedical implants [13,15].' Please, describe why these two references have been cited here, and add the most important information to the introduction section. The correct way to cite previous work includes some description of what the authors did, and what the conclusion was - so the reader knows how seriously to take the information you claim from them.

A: Introduction completely revised, as stated above (p. 4-6).

R: - Page 4, end of the first paragraph, it is stated that 'Cast alloys containing 27-30 wt% Cr and 5-7wt% Mo are biocompatible and have been used for many years to produce medical implants'. Have these data been obtained from a previous study? If so, please, include the reference.

A: This result was obtained in a previous study and the reference to it is added as ref [15] of the manuscript.

R: - Page 4, paragraph two. Please, explain the reasons why '… objects realized by sintering metal powder show mechanical properties worse than those held by objects produced in a conventional way…'.

A: The explanation required and reference [22] are added (p. 5-6, l. 89-94).

R: - The purpose of the work has not been clearly defined. Even some results and conclusions are mixed when defining the purpose of the investigation.

A: The purpose of the work as well as the main results and the conclusions are rewritten in the Introduction (p. 6, l. 95-103)

R: - For clarity, characteristics of the raw materials should be stated in 'Section 2. Materials'. Information should be reordered for a better understanding: in page 8, SEM analyses of the raw material are mixed with XRD analysis of the samples developed by laser sintering.

A: Section 2 "Materials and methods" and Section 3 "Results" are divided in subsections. The results obtained by each different characterisation technique are reported separately (p. 6-17).

R: - Was the composition of the raw material provided by the manufacturer? If so, please, state it. How was it manufactured? Is the chemical composition in agreement with some specification for powders to be used for surgical and medical implant coatings?

A: The nominal composition of the raw material (powder) was provided by the manufacturer (EOS GmbH Electro Optical Systems). The powder is the EOS Cobalt/Chrome SP2 cobalt based metal ceramic alloy intended for production of Porcelain-Fused to Metal (PFM) dental restorations (crowns, bridges, etc.) in EOSINT M 270 Standard installation mode. The powder is class IIa medical device in accordance with annex IX rule 8 of the MDD 93/42/EEC. Composition corresponds to "type 4" CoCr dental material according to EN ISO 22674. Information added in manuscript (p. 7, l. 111-118).

R: - How was the average particle size determined?

A: The average particle size is determined from SEM images. A sentence on this specific issue is added in Section 3.3 "Scanning electron microscopy (SEM) and microanalysis (EDS)" (p. 11, l. 187-189).

R: - Page 5. Methods. Were the parameters selected for the Laser Melting Sintering Process based on previous results?

A: The deposition parameters adopted for the laser sintering are the standard parameters recommended by the manufacturer.

R: - Page 5, first line: Using the passive voice would be more appropriate than the Active form 'We investigated…'.

A: Modified as suggested (p. 6, l. 95-97).

R: - Section 2, page 6. Please complete the information on the working conditions of the XRD equipment, that is: kV, mV and the range of 2θ degrees in which the test was performed.
A: The required information is added (p. 8, l. 133-134).

R: - Page 14, section 4: 'The hardness values of the laser sintered samples are surprisingly good, considering the method used for their realization. Generally, components produced by an additive manufacturing technique, such as the Direct Laser Metal Sintering procedure used in this work, can be affected by residual porosity and show poorer mechanical properties than those obtained with traditional manufacturing techniques. In our case, however, hardness was found to be remarkably high…'.

Are the high hardness values obtained good for biomedical applications? Is it associated to brittleness? Please, discuss it.
A: Section 4 "Discussion" is modified on the basis of the reviewer comments. Further comments on the mechanical parameters influencing the material behaviour are added (p. 17-18, l. 280-289).

R: If mechanical properties tend to be poorer in samples produced by Direct Metal Sintering, should the hardness values also diminish? If their increase is attributed to martensitic transformations, is there any way to reduce the hardness values of the obtained samples? Please, discuss these issues and place the obtained results into the context of literature.
A: Aim of this work is to correlate the hardness value measured on the samples to their microstructure. The complete determination of the mechanical behaviour of the samples is beyond the scope of the work. Future work on the same materials will take into consideration more mechanical aspects. Comments on this issue are added at the end of the "Discussion" (p. 22, l. 384-387).

R: - Are there other proposals that might usefully be tested in future work?
A: A list of possible issues to be explored is reported at the end of the "Discussion" (p. 22, line 379-382).

R: - References: some references date from year 1992, 1990, 1983, 1982, 1981, 1976, 1968 or even 1950. Even if correct, they may be hardly remarkable for a scientific paper. Please replace some of them with proper references from the open literature.
A: References were updated (p. 23-26).

Reviewer #3: In this paper, the authors used direct Metal Laser Sintering (DMLS) technique to sinter metal powder particles. During their processing, they found a homogeneous microstructure comprised of thin <epsilon>(hcp)-lamellae distributed inside a <gamma>(fcc) phase. It's hoped that this structure would prevent the dislocation slip and increase the sample hardness. With this structure, DMLS is expected to fabricate a useful computer-aid-designed three dimensional object with proper mechanical property for medical applications. This is an interesting result. However, the paper should provide more details.

R:(1) Hardness only reflects one aspect of the material mechanical property. The main mechanical property considering for the medical metal implants is the compression or intension property. There are somewhat big differences between the hardness and compression/intension. The author implied in the paper the structure is useful to improve the hardness, but not mentioned if that is benefit to improve the compression or intension property.

A: Aim of this work is to correlate the hardness value measured on the samples to their microstructure. The complete determination of the mechanical behaviour of the samples is beyond the scope of the work. Future work on the same materials will take into consideration more mechanical parameters and the mechanical properties required for biomedical applications. Comments on this issue are added at the end of the "Discussion" (p. 22, l. 384-387).

R: (2) The introduction part should provide more information about the current progress on the topic of the material structure developed by the DMLS or related technique, but not the background of the rapid manufacture and cobalt based alloy.

A: Introduction has been deeply modified following the reviewer suggestions. New and updated references have been added [20, 21]. The original results presented in the paper are summarised both in the Abstract (p. 3, l. 36-40) and in the Introduction (p. 6, l. 95-103).

R: (3) If the powder was commercially brought, it is needed to provide the powder manufacture's name and the grades.

A: The raw material is a commercial powder provided by EOS GmbH Electro Optical Systems. The powder is the EOS Cobalt/Chrome SP2 cobalt based metal ceramic alloy intended for production of Porcelain-Fused to Metal (PFM) dental restorations (crowns, bridges, etc.) in EOSINT M 270 Standard installation mode. The powder is class IIa medical device in accordance with annex IX rule 8 of the MDD 93/42/EEC. Composition corresponds to "type 4" CoCr dental material according to EN ISO 22674. Information added in manuscript (p. 7, l. 111-118).

R: (4) Fig. 1b, ordinate values of Y axis should be presented. Fig 1 should put the XRD pattern of sample fabricated by the traditional method.

A: Figure 1b is modified, as suggested: the Y scale is added (p.9). Figure 1 reports the experimental results obtained in this study by XRD. We experimentally performed XRD measurements on the raw material (powder) and the sintered samples. So, we reported these results in the "Results"

section of the manuscript in Figure 1a and Figure 1b, respectively. The XRD patterns of samples fabricated by traditional methods can be found in literature.

R: (5) Fig. 2, the bar size is 50 um, the biggest powder in the SEM image is about 60 um. However, the author describe the "…They have a spherical shape and size range from 4 to 90 um.…". It's look like the description and the image is inconsistent.

A: The average particle size is determined from SEM images by averaging the data obtained from several areas. Results show that the particle size is within the range 4-80 μm. A sentence on this specific issue is added in Section 3.3 "Scanning electron microscopy (SEM) and microanalysis (EDS)" (p. 11, l. 187-189).

R: (6) Page 9, "EDX measurements performed…", page 11 "EDX measurements performed…", page14 "EDX measurements were…", but, no EDX results are found in the paper.

A: The results of the EDX measurements are now added. Table 2, added in subsection 3.3 (p. 11), reports the EDX results obtained on the raw material (powder) and the sintered sample. Table 3, added in the subsection 3.4 (p.17), reports the EDX results obtained on the matrix (sintered sample) and the precipitates (metal carbides) visible in the TEM image reported in Figure 6.

R: (7) Page 8, "resulted in an <epsilon>-phase volume fraction fhcp=0.49±0.03", Page 11, " The<epsilon> phase forms lamellae inside the <gamma> phase…". if the volume fraction of<epsilon>-phase is almost the main phase, the description in page 11 should be changed.

A: The experimental results show that the epsilon phase is not present in the raw material (powder) while it is largely present in the sintered samples (see XRD results reported in Figure 1 and TEM results reported in Figure 4 and Figure 5). It must be considered that epsilon is the stable phase at low temperature while gamma is the stable phase at high temperature. Therefore, since DMLS induces the melting of the powder, the epsilon phase forms as a consequence of the gamma-epsilon martensitic transformation. So, the epsilon phase forms inside the gamma phase, as reported in the "Discussion".

Reviewer #5: This research paper reported the structural and microstructural characterization of Co-Cr-Mo parts produced by Direct Metal Laser Sintering. The method used is quite conventional, however, the results are a little valuable. It is obvious that this paper is not that well organized. Some minor revision must be taken.

R: 1. Please include an "Highlights section"
A: The highlights session is added (p. 2).

R: 2. The "M&M" and "Results" parts should be organized in sub-units, each used technique has to be described separately and consequently numbered.
A: Section 2 "Materials and methods" and Section 3 "Results" are divided in subsections. The results obtained by each different characterisation technique are reported separately (p. 6-17).

R: 3. The authors show an increase in Cr and Mo concentrations with respect to the matrix and evidence that precipitates have the same composition independently of their shape. Crystallographic examination of the precipitate was done by SAD technique. How to prove the biocompatibility of such precipitates?
A: The formation of the metal carbides in alloys having a composition similar to the alloy investigated in this work is well known in literature. From a compositional point of view, the sintered samples obtained by DMLS in this study are very similar to alloys reported as biocompatible materials in literature. Furthermore, the dimension and density of the metal carbides in our samples are comparable and sometimes even lower than those reported in several papers in literature. Therefore, even though a specific study on the biocompatibility of our samples was not performed, it is reasonable to consider the sintered samples of our study as biocompatible materials.

R: 4. P15: "Generally, components produced by an additive manufacturing technique, such as the Direct Laser Metal Sintering procedure used in this work, can be affected by residual porosity and show poorer mechanical properties than those obtained with traditional manufacturing techniques." Please add any references.
A: On this specific issue ref [22] is added.